Digital Object Identifier (DOI): 10.1109/IECON.2015.7392671

Industrial Electronics Society, IECON 2015 - 41st Annual Conference of the IEEE; November 2015

Design of a grid adaptive controller for PWM converters with LCL filters

Markus Andresen
Marco Liserre
Friedrich W. Fuchs
Nils Hoffmann

Suggested Citation

M. Andresen, M. Liserre, F. W. Fuchs and N. Hoffmann, "Design of a grid adaptive controller for PWM converters with LCL filters," *Industrial Electronics Society, IECON 2015 - 41st Annual Conference of the IEEE*, Yokohama, 2015, pp. 003664-003671.

Design of a Grid Adaptive Controller for PWM Converters with LCL Filters

Markus Andresen, Marco Liserre, Friedrich W. Fuchs
Chair of Power Electronics
Christian-Albrechts-Universität zu Kiel
Kiel, Germany

Nils Hoffmann
R&D, Power Electronics and Electrical Drives
Ingenieurbüro Hoffmann GmbH
Halle/Saale, Germany

***Abstract*—The system resonance frequency of a grid connected inverter with LCL filter depends on the filter parameters and the time varying grid impedance. To obtain stability and to preserve good dynamic behavior of the system, grid impedance adaptation of the current controller is proposed. The design of the current controller is described and the adaptation strategy to prevent the excitation of the system resonance frequency during grid-impedance changes is introduced. The actual grid impedance is estimated by an extended Kalman filter (EKF) and a Luenberger observer allows to use the same number of voltage and current sensors as in conventional PI controllers. The proposed control method provides the possibility to tune the controller dynamics independently from the grid impedance. The theoretical analysis is validated with laboratory measurements.**

Keywords—current control; LCL filter; grid impedance; PWM converter

I. INTRODUCTION

Grid-connected PWM voltage source converters with LCL filters are widely used to feed decentralized produced energy into the electrical distribution grid [1]. The time-variable penetration of energy affects a varying utilization of the lines and nodes in the distribution grid and impacts the stability of the connected systems [2]. The variations in the energy production lead to varying grid impedances, which are seen from the inverter to the distribution grid. Therefore, the parameter of the overall grid side inductance, necessary to tune the current controller, changes. The result is improper controller tuning, which results in reduced dynamics or even instability and increased harmonics in the grid currents [3],[4].

Commonly, proper current control of grid connected converters is ensured by introducing proportional-integral (PI) controllers, which are designed to be robust against parameter variations. Nevertheless, the frequently used voltage oriented control scheme with PI-based current controllers is limited to certain ratios between the control frequency and the filter resonance frequency as analyzed in [5].

To expand the limits of operation, a current controller with additional state feedbacks is a possible solution [6]. The additional state feedback is also used for active damping of the LCL filter resonance frequency [7]-[12]. Additionally, active damping with full state feedback reduces the effect of grid impedance variations on the system behavior compared to actively damped systems with partial state feedback [13]-[15]. In the literature, several tuning procedures have been presented for the state space approach with full state feedback. Examples are the linear-quadratic regulator [16], the equivalent L-Filter design [14], deadbeat control [8] or pole placement strategies [17]. Recent work has used the state space approach to implement a robust controller [18],[19] or to examine the stability of the control approach [20]. Furthermore, a state space approach has been presented with a Luenberger observer under consideration of coupling effects of the state variables [21]. Disadvantageous for full state feedback is the need to determine all state variables, which increases the system costs significantly if every state is measured. Another approach to reduce the number of sensors is using observer based state estimation techniques [22]-[24].

For the determination of the equivalent grid impedance, offline measurement methods or online solutions can be applied [19]. An approach to adapt a varying grid impedance in a state space controller has been presented in [21] with a model reference adaptive system (MRAS), while in [25] a grid impedance adaptation is realized with a feed forward control of the grid voltage.

The purpose of this work is to design and analyze a grid impedance adaptive current controller, which enables converter control performance almost independently from grid impedance variations. Therefore, the actual time variable grid impedance is considered in the design of a state space controller and during operation it is estimated by means of an extended Kalman-Filter (EKF). For increased robustness against parameter uncertainties a PI-based pre-filter is used in addition to a state space current controller. A Luenberger observer is designed for sensor reduction and the performance of the resulting controller in a model identification adaptive system (MIAS) system is analyzed and presented.

This paper first describes the system and the control approach in section II and the adaptation via pole placement and the observer design is shown in chapter III. In section IV a measurement study is carried out. The paper is closed with a conclusion in the last chapter.

II. SYSTEM DESCRIPTION AND MODELING

In Fig. 1 a model of the system including the signal flow chart is shown. It consists of a two-level voltage-source inverter (VSI), which is connected to the grid, with an LCL filter. The grid is modeled via a Thevénin equivalent. To provide information about the grid-condition to the current

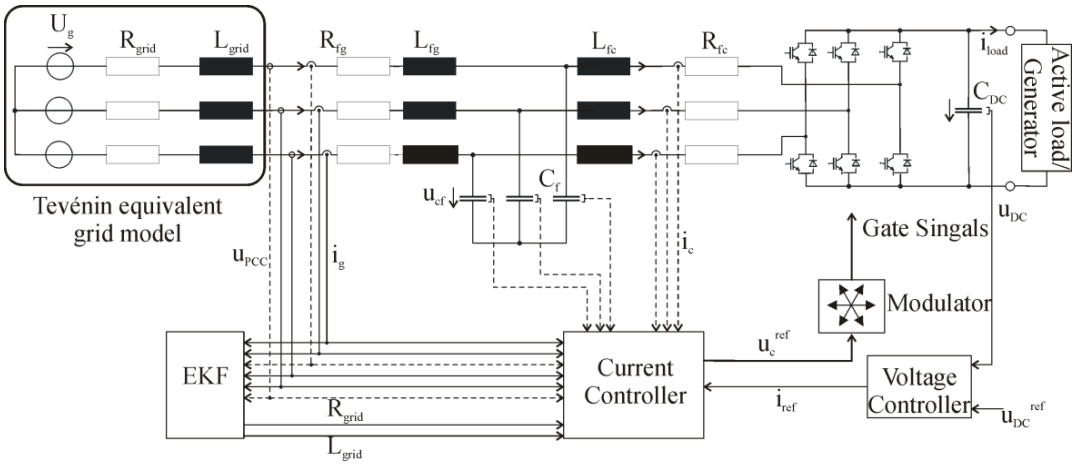

Fig. 1: Block diagram of the grid connected inverter with a LCL filter.

controller, an EKF estimates the equivalent grid impedance. The block diagram already indicates which states are measured (solid sensor lines) and which are observed (dashed sensor lines). Based on this model a state space formulation is derived for the controller design. The state vector consists of the grid side currents $\vec{\imath}_g^{\alpha\beta}(t)$, the inverter side currents $\vec{\imath}_c^{\alpha\beta}(t)$ and the filter capacitor voltage $\vec{u}_{cf}^{\alpha\beta}(t)$. The control vector consists of the inverter voltage $\vec{u}_c^{\alpha\beta}(t)$ and the equivalent grid voltage $\vec{u}_g^{\alpha\beta}(t)$. To simplify the model formulation the grid side filter inductor and the grid-inductance are summarized to:

$$L_g = L_{fg} + L_{grid} \tag{1}$$

The equivalent resonance frequency f_{res} and the equivalent anti-resonance frequency f_0 of the LCL filter system depend on the grid inductance L_{grid}, the filter inductors L_{fc} and L_{fg} and the filter capacitor C_f:

$$f_{res} = \frac{1}{2\pi}\sqrt{\frac{L_{fc} + L_{fg} + L_{grid}}{C_f \cdot L_{fc} \cdot (L_{grid} + L_{fg})}}$$
$$f_0 = \frac{1}{2\pi}\sqrt{\frac{1}{C_f \cdot (L_{grid} + L_{fg})}} \tag{2}$$

The resistive elements in the filter model only cause inherent damping of the LCL filter state variables. Therefore a state space formulation, which is limited to the reactive parts, considers the worst case scenario for the stability and is taken here. The discretization is carried out utilizing the zero-order hold (zoh) equivalent discretization method with a sampling frequency $f_{con} = 1/T_{con}$. The according PWM time-delay of the inverter output voltage $\vec{u}_c^{\alpha\beta}$ to the reference signal $\vec{u}_{ref}^{\alpha\beta}$ in the discrete time domain is presented in (3).

$$\vec{u}_c^{\alpha\beta}(k+1) = \vec{u}_{ref}^{\alpha\beta}(k) \tag{3}$$

The resultant system description with the grid voltage $\vec{u}_g^{\alpha\beta}$ is summarized in (4).

III. Control Strategy

The voltage oriented control strategy with an outer DC-link voltage controller and an inner current controller is used to control the grid-connected VSI with LCL filter. Thereby the DC-link voltage controller is a PI controller tuned with the symmetrical optimum similar to [21]. The inner current control is implemented as a PI state space controller.

$$\underbrace{\begin{bmatrix} \vec{i}_g^{\alpha\beta}(k+1) \\ \vec{i}_c^{\alpha\beta}(k+1) \\ \vec{u}_{cf}^{\alpha\beta}(k+1) \\ \vec{u}_c^{\alpha\beta}(k+1) \end{bmatrix}}_{\vec{x}^{\alpha\beta}(k+1)} = \underbrace{\begin{bmatrix} a_{11} & a_{12} & a_{13} & b_{11} \\ a_{21} & a_{22} & a_{23} & b_{21} \\ a_{31} & a_{32} & a_{33} & b_{31} \\ 0 & 0 & 0 & 0 \end{bmatrix}}_{A_{O1}} \cdot \underbrace{\begin{bmatrix} \vec{i}_g^{\alpha\beta}(k) \\ \vec{i}_c^{\alpha\beta}(k) \\ \vec{u}_{cf}^{\alpha\beta}(k) \\ \vec{u}_c^{\alpha\beta}(k) \end{bmatrix}}_{\vec{x}^{\alpha\beta}(k)}$$
$$+ \underbrace{\begin{bmatrix} 0 & b_{12} \\ 0 & b_{22} \\ 0 & b_{32} \\ 1 & 0 \end{bmatrix}}_{B_{O1}} \cdot \underbrace{\begin{bmatrix} \vec{u}_{ref}^{\alpha\beta}(k) \\ \vec{u}_g^{\alpha\beta}(k) \end{bmatrix}}_{\vec{u}^{\alpha\beta}(k)} \tag{4}$$

A. PI State Space current Control

Based on the concept of state space control, the PI state space control is an extension, whereas the control-loops pre filter is replaced by a PI controller [14]. This leads to the advantage that parameter variations or parameter uncertainties do not result in a steady-state control deviation. Furthermore, it provides the tuning of one more parameter for determining the closed loop behavior. The structure of PI state space control is shown in Fig. 2. In addition to the controller a Luenberger observer is implemented to reduce the number of voltage and current sensors needed. In the block diagram k_F is the controller feedback vector and k_{OP} is the observer feedback vector. The controller is designed in the rotating dq-reference frame, which requires a transformation of the state variables accordingly. The Park transformation is expressed for an arbitrary variable in the stationary αβ-reference frame $\phi^{\alpha\beta}(k)$ with the grid frequency f_N:

$$\phi^{dq}(k) = \phi^{\alpha\beta}(k) \cdot \exp\{-j2\pi f_N k T_{con}\} \tag{5}$$

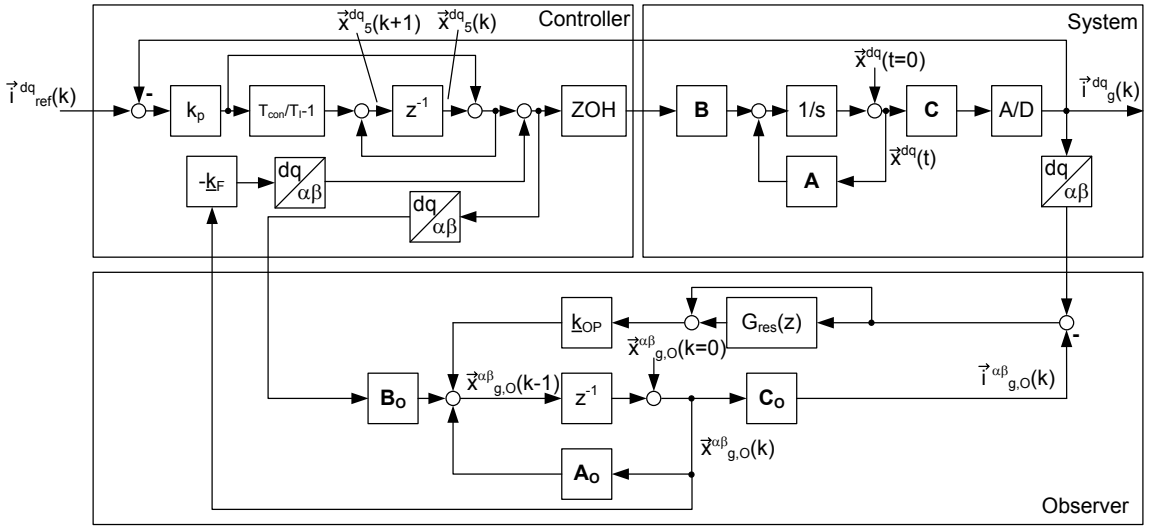

Fig. 2 Block diagram for PI state space current control with Luenberger Observer.

The dq transformation introduces a cross-coupling between the d- and q-component of the state variables. Especially the coupling caused by the time-delay is crucial.

This problem is addressed in [21] and is overcome with:

$$\phi^{\mathrm{dq}}(\mathrm{k}+1) = \phi^{\mathrm{dq}}(\mathrm{k}) \cdot \underbrace{\exp\{-\mathrm{j}2\pi \mathrm{f_N} \mathrm{T_{con}}\}}_{\mathrm{r}} \tag{6}$$

After applying the Park-transformation and the decoupling of the inverters time delay (6) to the state space model (4), the complex-valued state space formulation with the output variable $\vec{\imath}_g^{dq}(k)$ results in:

$$\begin{aligned}\vec{\mathrm{x}}^{\mathrm{dq}}(\mathrm{k}+1) = \underbrace{\mathrm{A_{O1}} \cdot \mathrm{r}}_{\mathrm{A}} \cdot \vec{\mathrm{x}}^{\mathrm{dq}}(\mathrm{k}) + \underbrace{\mathrm{r} \cdot \begin{bmatrix}0\\0\\0\\1\end{bmatrix}}_{\mathrm{B}} \cdot \vec{\mathrm{u}}_{\mathrm{ref}}^{\mathrm{dq}}(\mathrm{k}) \\ + \mathrm{r} \begin{bmatrix}\mathrm{b_{12}}\\ \mathrm{b_{22}}\\ \mathrm{b_{32}}\\ 0\end{bmatrix} \cdot \vec{\mathrm{u}}_{\mathrm{g}}^{\mathrm{dq}}(\mathrm{k})\end{aligned} \tag{7}$$

$$\vec{\mathrm{y}}^{\mathrm{dq}}(\mathrm{k}) = \underbrace{[1 \quad 0 \quad 0 \quad 0]}_{\mathrm{C}} \cdot \vec{\mathrm{x}}^{\mathrm{dq}}(\mathrm{k}) \tag{8}$$

For the current controller tuning, the PI pre filter is included in the state space model. The continuous transfer function $G_{PI}(s)$ with the proportional gain k_p the integration time T_I is shown in (9).

$$\mathrm{G_{PI}}(\mathrm{s}) = \mathrm{k_p} \cdot \left(1 + \frac{1}{\mathrm{T_I s}}\right) = \frac{\mathrm{Y(s)}}{\mathrm{U(s)}} \tag{9}$$

This transfer function is discretized with the Euler-forward numerical approximation, where *Y(z)* is the pre filter's output and *U(z)* is the pre filter's input. The discretization of this transfer function leads to (10).

$$\begin{aligned}\mathrm{Y(k+1)}|_{\mathrm{t=k \cdot T_{con}}} = \mathrm{Y(k)} + \mathrm{k_p} \cdot (\mathrm{u(k+1)} - \mathrm{u(k)} \\ + \frac{\mathrm{T_{con}}}{\mathrm{T_I}} \mathrm{u(k)})\end{aligned} \tag{10}$$

The state space formulation (7-8) is now extended with the integral part of the pre filter, where the integral part is chosen to a new state space variable. This leads to a new expression of the reference voltage $\vec{u}_{ref}^{dq}(k)$ (11) and a new expression for the integral output of the PI-based pre filter $\vec{x}_5^{dq}(k)$ with the output vector *C* (12).

$$\vec{\mathrm{u}}_{\mathrm{ref}}^{\mathrm{dq}}(\mathrm{k}) = \mathrm{k_p} \cdot \left(\vec{\mathrm{i}}_{\mathrm{ref}}^{\mathrm{dq}}(\mathrm{k}) - \mathrm{C} \cdot \vec{\mathrm{x}}^{\mathrm{dq}}(\mathrm{k})\right) + \vec{\mathrm{x}}_5^{\mathrm{dq}}(\mathrm{k}) \tag{11}$$

$$\begin{aligned}\vec{\mathrm{x}}_5^{\mathrm{dq}}(\mathrm{k}+1) = \vec{\mathrm{x}}_5^{\mathrm{dq}}(\mathrm{k}) + \mathrm{k_p} \cdot \frac{\mathrm{T_{con}}}{\mathrm{T_I}} \left(\vec{\mathrm{i}}_{\mathrm{ref}}^{\mathrm{dq}}(\mathrm{k}) - \mathrm{C} \cdot \right. \\ \left. \vec{\mathrm{x}}^{\mathrm{dq}}(\mathrm{k})\right)\end{aligned} \tag{12}$$

The resulting state space model now completely covers the system including the state space controller with the PI-based pre filter (13). This formulation is advantageous, because the calculation of the characteristic polynomial, describing the dynamic system behavior, is straightforward.

$$\begin{aligned}\begin{bmatrix}\vec{x}^{dq}(k+1)\\ \vec{x}_5^{dq}(k+1)\end{bmatrix} = \underbrace{\begin{bmatrix}A - BK_F - k_pBC & B\\ -k_p\frac{T_{con}}{T_I}C & 1\end{bmatrix}}_{A_{ges}} \\ \cdot \begin{bmatrix}\vec{x}^{dq}(k)\\ \vec{x}_5^{dq}(k)\end{bmatrix} + \begin{bmatrix}k_pB\\ k_p\frac{T_{con}}{T_I}\end{bmatrix} \\ \cdot \vec{\imath}_{ref}^{dq}(k)\end{aligned} \tag{13}$$

For the state space controller tuning six tuning parameters are available to place five poles and one zero. The zero z_w only depends on the integral time of the equivalent PI controller and is freely placed by applying:

$$\mathrm{T_I} = \frac{\mathrm{T_{con}}}{\mathrm{z_w} - 1} \tag{14}$$

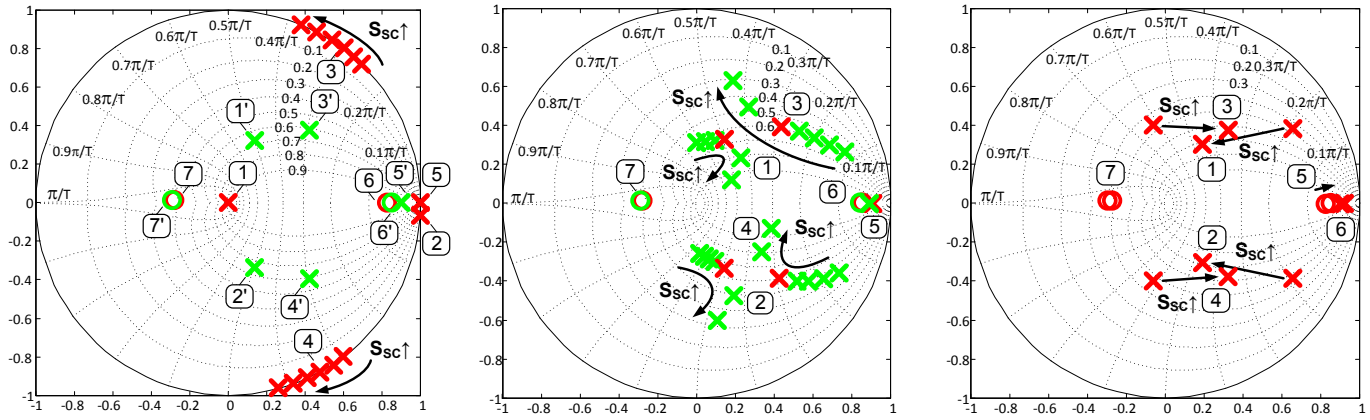

(a) (b) (c)

Fig. 3: Pole zero maps with parameters from Table I: (a) Open loop poles and zeros $S_{SC} = 221\ pu \ldots 6.58\ pu, X/R = inf$ (red x) and inserted closed loop poles and zeros (green x) $S_{SC} = 33{,}95\ pu, X/R = inf$ (b) Closed loop poles for varying grid impedances $S_{SC} = 221\ pu \ldots 6.58\ pu$, $X/R = inf$ and controller tuning for $S_{SC} = 33.95\ pu, X/R = inf$ (red x) and (c) Proposed closed loop adaptive pole placement strategy for $S_{SC} = 221\ pu \ldots 6.58\ pu, X/R = inf$.

The characteristic polynomial of the overall system which contains the controller poles is calculated with (15).

$$\mathrm{P(z)} = \det\left(\mathrm{zI} - \mathrm{A_{ges}}\right) \tag{15}$$

The characteristic polynomial is a function of the system parameters, the controller feedback vector and the PI pre filter parameters. The matrix I is the identity matrix. To specify the closed loop current control behavior the five poles of the system are placed freely. This is done with a coefficient comparison presented in (16), where p_{wi} with $i \in \{1,2,3,4,5\}$ are the desired complex pole positions.

$$\mathrm{P(z)} = (\mathrm{z} - \mathrm{p_{w1}})(\mathrm{z} - \mathrm{p_{w2}})(\mathrm{z} - \mathrm{p_{w3}})(\mathrm{z} - \mathrm{p_{w4}})(\mathrm{z} - \mathrm{p_{w5}}) \tag{16}$$

An analytical solution of (16) leads to unpractical terms caused by the high model complexity. Further, the complexity of these analytical derived terms is of such a high degree that it is not constructive to add them to the appendix of this manuscript.

B. Grid Impedance Adaptive Pole placement

The controllability of the system is proven in [26], which enables to force the system to obtain a desired dynamic behavior. In Fig. 3 (a) the open loop pole zero map (red x) is drawn for varying grid conditions (system parameters of Table I). The poles 3 and 4 represent the resonance frequency poles, which depend on the grid impedance. Similar, the system zeros (zero 7) depend on the grid impedance and cannot be manipulated by the controller. Pole 1 is caused by the PWM delay and pole 2 represents the ZOH element of the discretization. Pole 5 and zero 6 are introduced by the pre filter. Since the grid impedance influences the closed loop behavior an adaptive pole placement is developed for obtaining stability and a comparable system behavior despite varying grid conditions. The basic pole placement strategy in Fig. 3 (a) (green x) is described as follows: A complex conjugated pole pair (pole 1´, 2´) is placed on the anti-resonance frequency to reduce the influence of the system zeros (zero 6). The second complex conjugated pole pair (pole 3´, 4´) is set to affect the desired dynamical behavior.

TABLE I
Parameters of the theoretical analysis and the measurement system

Quantity	Notation	Value (per unit)
Line-to-line voltage	u_g	400 V (1.0)
DC-link voltage	u_{DC}	700 V (1.75)
Angular line frequency	ω_N	2π 50 Hz
Rated converter current	I_L	32 A (1.0)
Grid side filter inductance	L_{fg}	1 mH (0.043)
Converter side filter inductance	L_{fc}	3 mH (0.129)
Equivalent grid-inductance	L_{grid}	80 µH (0,004)
Equivalent grid-resistance	R_{grid}	327 mΩ (0.026)
Filter capacitance	C_f	32.4 µF (0.074)
DC-link capacitance	C_{DC}	2200 µF (5.0)
Control/Switching frequency	$f_{carrier}$ /f_{con}	5 kHz / 2.5 kHz (100/50)

In Fig. 3 (b) the controller is tuned for the short circuit power

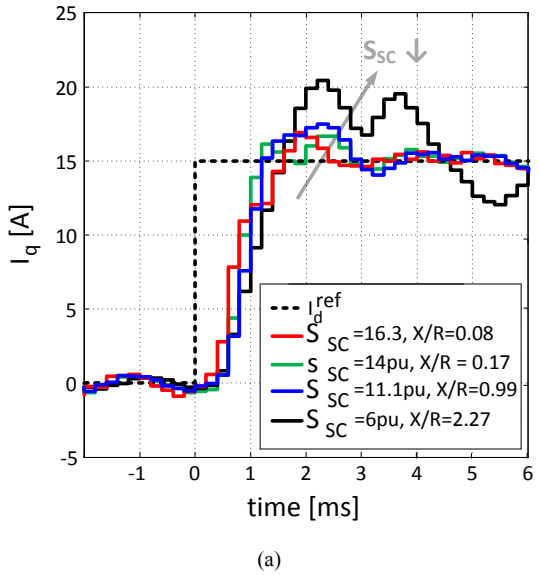

(a)

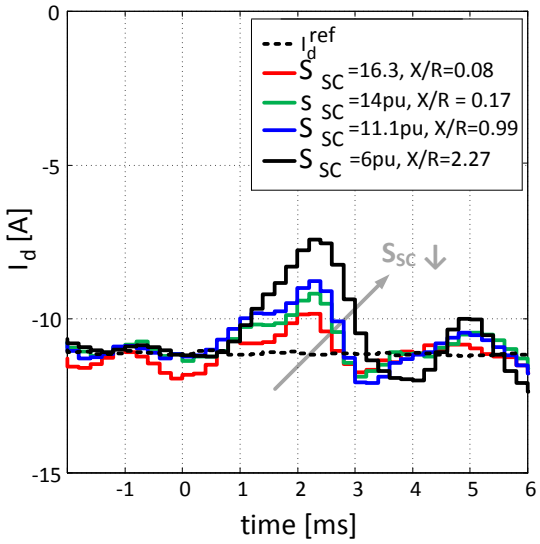

(b)

the gain margin is around zero and the bandwidth is highly reduced while the 5th harmonic is even amplified. Instead, the

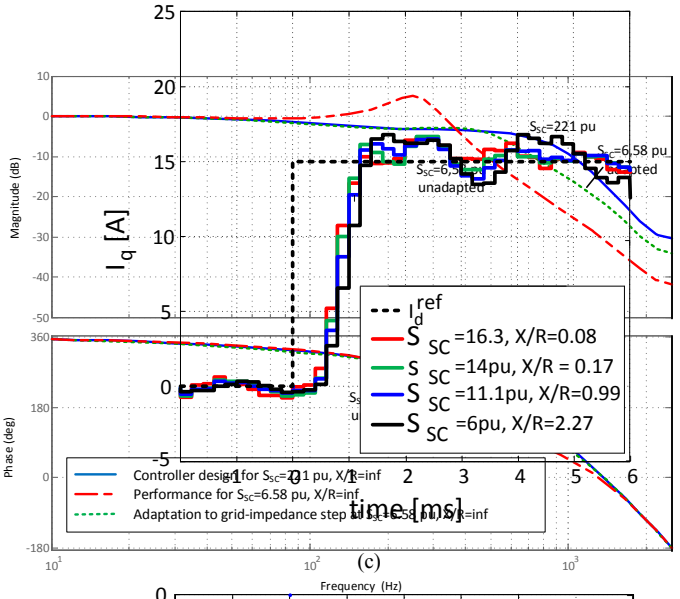

(c)

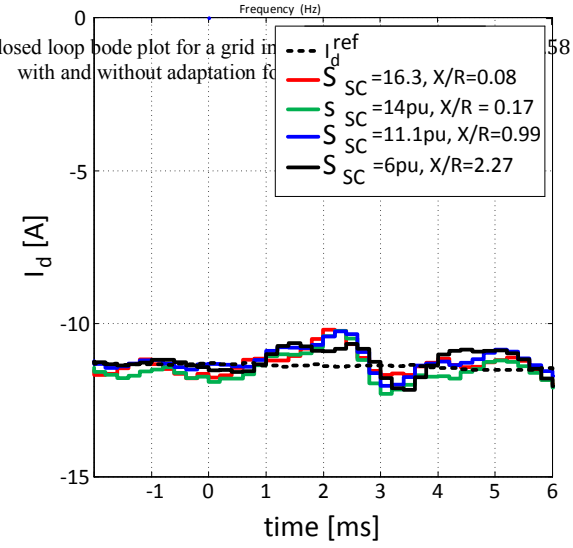

(d)

Fig. 4: Closed loop bode plot for a grid in … 58 pu with and without adaptation fo…

Fig. 5: Measurement: Comparison between adapted and unadapted controller behavior during reactive current steps: (a), (b) Tuned for $S_{SC} = 14\ pu$ ($L_{grid} = 0.025\ pu$) and (c), (d) adapted.

$S_{SC} = 33.95$ pu and the effect of higher and lower grid impedances without adaptation is illustrated. Even if the system stays stable for the presented variations the dynamics are changing and complex-valued. Thus, a coupling of d- and q-components remains. To overcome this non optimal controller behavior Fig. 3 (c) illustrates the proposed control adaptation strategy. The location of poles 1-5 and zeros expose the adapted pole placement strategy. The zero 6 is shifted closer to pole 5 to reduce the influence of pole 5 on the system behavior for increasing grid impedances. In parallel, the complex conjugated poles 1-4 dominate the system dynamic behavior.

To better demonstrate the effect of the adaptation, a bode plot is shown for the controller tuning for a strong grid ($S_{SC} = 226\ pu$) and a change in the grid impedance ($S_{SC} = 6{,}58\ pu$) with and without the adaptation strategy. Without the adaptation, adaptation shows a good fit in magnitude response and frequency response and a similar gain and phase margin.

The feedback vector and the parameters of the pre filter are calculated offline as a function of the grid impedance. For online implementation purposes the resultant function is approximated with a second order polynomial for the interval of expected grid impedance variation. The fit of the approximation is exemplarily shown for the proportional part of the pre filter k_P:

$$k_p = a_0 + a_1 \cdot L_{grid} + a_2 \left(L_{grid}\right)^2 \tag{17}$$

The parameters for the approximation and the mathematical expression for the pole placement strategy are summarized in Table III in the Appendix.

C. Grid Impedance Estimation with an Extended Kalman-Filter (EKF)

The equivalent grid impedance can either be estimated online with software-based solutions or measured with additional power electronic hardware [27]. Since the measurement solutions normally obtain poor dynamics they are not suitable for the purpose of an adaptive controller in an online manner. For this reason, an EKF is used for the online estimation of the equivalent grid impedance. Here, the noise that is already present at the point of common coupling (PCC) is used to perform online grid impedance estimation. A detailed explanation for the design procedure and a measurement study are presented in [19] and will not be further discussed in this work.

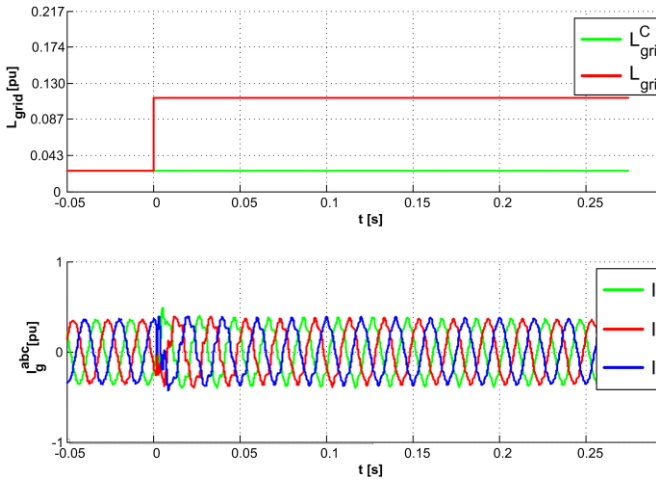

Fig. 6 Measurement: Grid side currents after grid-impedance step $L_{grid} = 0.025\ pu \rightarrow 0.112\ pu$ without controller adaptation.

D. P-Res Observer for Sensor Reduction

An observer is developed in the stationary reference frame for purpose of sensor reduction. The design is similar to the state space model in (7) but with changes according to (18-20).

$$\mathrm{A_O} = \mathrm{A_{O1}}(\mathrm{L_g} = \mathrm{L_{fg}}) \tag{18}$$

$$\mathrm{B_O} = \mathrm{B_{O1}}(\mathrm{L_g} = \mathrm{L_{fg}}) \tag{19}$$

$$\vec{\mathrm{u}}_{\mathrm{g}}^{\alpha\beta}(\mathrm{k}) = \vec{\mathrm{u}}_{\mathrm{PCC}}^{\alpha\beta}(\mathrm{k}) \tag{20}$$

The resulting system is observable for the measurement of grid side currents [16], which are also required to measure for the EKF. The observer is formulated in the stationary reference frame due to the occurring coupling effects in the rotating reference frame. To increase the robustness against parameter uncertainties a P-Res observer is introduced. The resonant part serves as an integral term, which is suggested in [28] for ensuring stationary precision in case of parameter changes or uncertainties of the LCL filter system. One critical aspect for the resonant controller tuning is the time delay caused by the systems sampling, control output calculation and PWM update routine. By applying (21) this delay is compensated and stability margins of the resonant controller are increased [29].

$$\mathrm{G_{Res}}(\mathrm{z}) = \mathrm{K_I}\frac{\mathrm{z}^2 \cdot \cos(2\omega_\mathrm{N}\mathrm{T_{con}}) - \mathrm{z}\cos(\mathrm{N}\omega_\mathrm{N}\mathrm{T_{con}})}{\mathrm{z}^2 - 2\mathrm{z}\cos(\omega_\mathrm{N}\mathrm{T_{con}}) + 1} \tag{21}$$

This leads to the observer feedback vector with the proportional feedback vector $\underline{k}_{OP}$.

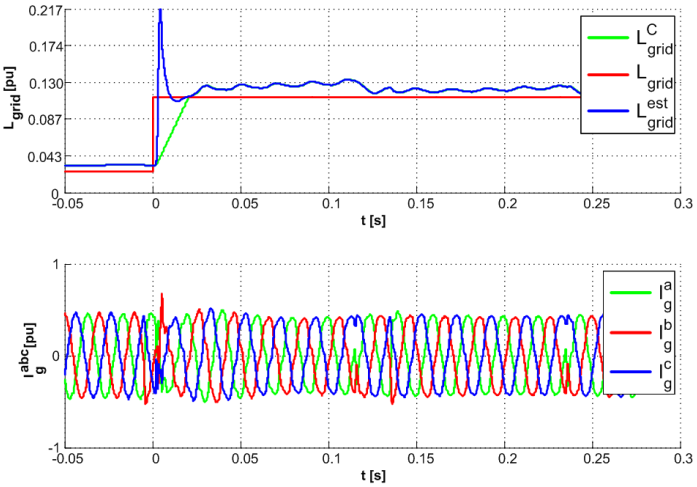

Fig. 7 Measurement: Grid side currents with PRBS signal after grid-impedance step $\mathrm{L_{grid}} = 0.025\ \mathrm{pu} \rightarrow 0.112\ \mathrm{pu}$ with controller adaptation and grid-impedance estimation.

$$\underline{\mathrm{k}}_\mathrm{O}(\mathrm{z}) = [1 + \mathrm{G_{Res}}(\mathrm{z})\,] \cdot \underline{\mathrm{k}}_\mathrm{OP} \tag{22}$$

IV. Experimental Results

The experimental validation is carried out on a 30 kVA laboratory test setup consisting of a two-level back-to-back voltage source inverter with an LCL filter. Table I presents a summary of the system parameters. Active load conditions are emulated by an inverter fed permanent-magnet synchronous machine (PMSM) connected to a DC load machine. During the tests the speed of the PMSM is set to $N = 1400\ min^{-1}$ and active power $P = -5\ kW$ is fed into the grid. A dSpace DS1006 system is used to perform the control algorithms.

A. Evaluation for constant grid conditions

Reactive current steps of 15 A are performed under several grid conditions to evaluate the steady state controller behavior. First the effects of grid impedance changes are shown for an unadapted controller and later the improvement achieved by the adaptation is shown. The results are presented in Fig. 5. No adaptation is applied for (a) and (b) while the controller is always tuned for $S_{SC} = 14\ pu\ (L_{grid} = 0.025\ pu)$. For the q-component a weaker grid leads to a longer rise time, while a stronger grid leads to an increased overshoot. The deviation of the d-component to its reference value after the step increases with the grid impedance. In contrast to this behavior, the adapted controller shows a smooth behavior independent from the grid impedance for the d-component as well as the q-component, see Fig. 5 (c) and (d).

B. Evaluation for varying grid conditions

The transient controller behavior is evaluated by grid impedance steps $L_{grid} = 0.025\ pu \rightarrow 0.112\ pu$. In Fig. 6 the

grid conditions change without adaption, leading to harmonics in the output spectrum, even if stability is maintained. The harmonics are still visible in the spectrum after more than 10 fundamental periods. In Fig. 7 the adaptation of the grid impedance estimated by the EKF is shown. For an improved detection of the varying grid impedance, an additional pseudo random biased signal (PRBS) is added on the q-component of the currents and causes the variations in the currents. Furthermore, the inductance L_{grid}^{C}, which is used for the tuning of the feedback vector is the filtered estimation of the Kalman filter $\mathrm{L}_{\mathrm{grid}}^{\mathrm{est}}$ to avoid oscillations caused by the stepwise change of the feedback vector. The adaptation is applied for $\Delta L_{grid}^{est} = 0.00086\ pu$ with:

$$\begin{aligned} \mathrm{L}_{\mathrm{grid}}^{\mathrm{C}} &= \mathrm{L}_{\mathrm{grid}}^{\mathrm{est}} \quad \text{for } \left|\mathrm{L}_{\mathrm{grid}}^{\mathrm{C}} - \mathrm{L}_{\mathrm{grid}}^{\mathrm{est}}\right| \le \Delta\mathrm{L}_{\mathrm{grid}}^{\mathrm{est}} \\ \mathrm{L}_{\mathrm{grid}}^{\mathrm{C}} &= \mathrm{L}_{\mathrm{grid}}^{\mathrm{est}} + \Delta\mathrm{L}_{\mathrm{grid}}^{\mathrm{est}} \text{ for } \mathrm{L}_{\mathrm{grid}}^{\mathrm{C}} - \mathrm{L}_{\mathrm{grid}}^{\mathrm{est}} < -\Delta\mathrm{L}_{\mathrm{grid}}^{\mathrm{est}} \\ \mathrm{L}_{\mathrm{grid}}^{\mathrm{C}} &= \mathrm{L}_{\mathrm{grid}}^{\mathrm{est}} - \Delta\mathrm{L}_{\mathrm{grid}}^{\mathrm{est}} \text{ for } \mathrm{L}_{\mathrm{grid}}^{\mathrm{C}} - \mathrm{L}_{\mathrm{grid}}^{\mathrm{est}} > \Delta\mathrm{L}_{\mathrm{grid}}^{\mathrm{est}} \end{aligned} \quad (23)$$

The EKF correctly estimates the grid impedance after approximately half a fundamental period. It needs to be pointed out, that the estimation of the EKF in the current version shows an offset, which is independently from the grid conditions. Contrary to the unadapted case, the visible harmonics in the output spectrum are rejected well after 5 fundamental periods and even the PRBS signal does not affect new distortion.

V. CONCLUSION

Variations in the grid impedance affect the stability and the dynamic performance of grid connected PWM converters. An adaptation of the grid impedance in a state space based current controller for grid connected PWM converters is presented to overcome the stability problems and to obtain controller behavior independently from the grid impedance. The controller design is shown and the tuning is described in detail. Experimental results demonstrate similar behavior during reactive current steps of the proposed controller despite different grid conditions. Improved behavior for an adaptation of the equivalent grid impedance in case of grid impedance steps is demonstrated.

ACKNOWLEDGMENT

These results have been worked out in the research project "Grid-Adaptive Control and Active Filter Functionality of Grid-Side PWM Converters in wind turbine applications" at the University of Kiel. The authors gratefully acknowledge the funding of this project by the European Union and the State of Schleswig-Holstein.

VI. APPENDIX

The coefficients of the state space model are summarized in Table II and in Table III the parameters for the approximated state feedback are presented.

TABLE II

Coefficients of the state space model

$a_{11} = \frac{L_g}{L_g + L_{fc}} + \frac{L_{fc} \cdot \cos(\omega_{res} T_{con})}{L_g + L_{fc}}$	$a_{12} = \frac{2L_{fc} \cdot \sin^2(\frac{\omega_{res} T_{con}}{2})}{L_g + L_{fc}}$	$a_{13} = -\frac{\sin(\omega_N T_{con})}{\omega_{res} L_g}$
$a_{21} = \frac{2L_g \cdot \sin^2(\frac{\omega_{res} T_{con}}{2})}{L_g + L_{fc}}$	$a_{22} = \frac{L_{fc}}{L_{fc} + L_g} + \frac{L_g \cdot \cos(\omega_{res} T_{con})}{L_g + L_{fc}}$	$a_{23} = \frac{\sin(\omega_{res} T_{con})}{\omega_{res} L_{fc}}$
$a_{31} = \frac{sin(\omega_{res} T_{con})}{\omega_{res} C_f}$	$a_{32} = -\frac{sin(\omega_{res} T_{con})}{\omega_{res} C_f}$	$a_{33} = \cos(\omega_{res} T_{con})$
$b_{11} = \frac{\sin(\omega_{res} T_{con})}{\omega_{res}(L_g + L_{fc})} - \frac{T_{con}\omega_{res}}{\omega_{res} C_f}$	$b_{21} = -\frac{L_g sin(\omega_{res} T_{con})}{\omega_{res} L_{fc}(L_g + L_{fc})} - \frac{T_{con}\omega_{res} L_{fc}}{\omega_{res} L_{fc}(L_g + L_{fc})}$	$b_{31} = \frac{2 \cdot \sin^2\left(\frac{\omega_{res} T_{con}}{2}\right)}{L_{fc} + L_g} \cdot L_g$
$b_{12} = \frac{T_{con}}{L_g + L_{fc}} + \frac{L_{fc}}{\omega_{res} L_g (L_{fc} + L_g)} \cdot si\,\mathrm{n}(\omega_{res} T_{con})$	$b_{22} = \frac{T_{con}}{L_g + L_{fc}} - \frac{si\,\mathrm{n}(\omega_{res} T_{con})}{\omega_{res}(L_{fc} + L_g)}$	$b_{32} = 2L_{fc} \sin(\frac{\omega_{res} T_{con}}{2})$

TABLE III

Coefficients of the feedback vector

	a_2	a_1	a_0
k_p	45068+7138j	-1665-264j	-4.69-0.74j
k_{ig}	-705300+61495j	35525-46j	3.05+0.01j
k_{ic}	604420-72411j	-6130+527j	-7.71+0.88j
k_{ufc}	-98271+8258j	606-114j	-1.52+0.15j
k_{uc}	-19031+2565j	255-9j	0.72-0.06j

REFERENCES

[1] R. Teodorescu, M. Liserre and P. Rodriguez, "Grid Converters for Photovoltaic and Wind Power Systems," *Wiley- IEEE Press*, 2011.

[2] M. Liserre, R. Teodorescu and F. Blaabjerg, "Stability of photovoltaic and wind turbine grid-connected inverters for a large set of grid impedance values," *IEEE Trans. on Power Electron.*, vol. 21, pp. 263-272, Jan. 2006.

[3] Y. Shuitao, L. Qin, F.Z. Peng and Q. Zhaoming, "A Robust Control Scheme for Grid-Connected Voltage-Source Inverters," *IEEE Trans. on Ind. Electron.*, vol. 58, pp. 201-212, Jan. 2011.

[4] S. Cobreces, E.J. Bueno, D. Pizarro, F.J. Rodriguez and F. Huerta, "Grid Impedance Monitoring System for Distributed Power Generation Electronic Interfaces," *IEEE Trans. on Instrum. and Meas.*, vol. 58, pp. 3112-3121, Sept. 2009.

[5] J. Dannehl, C. Wessels and F.W. Fuchs, "Limitations of Voltage-Oriented PI Current Control of Grid-Connected PWM Rectifiers with LCL-Filters," *IEEE Trans. on Ind. Electron.*, vol. 56, pp. 380-388, Feb. 2009.

[6] N. He, D. Xu, Y. Zhu, J. Zhang, G. Shen, Y. Zhang, J. Ma and C. Liu, "Weighted Average Current Control in a Three-Phase Grid Inverter With an LCL Filter," *IEEE Trans. on Ind. Electron.*, vol. 28, pp. 2785-2797, June 2013.

[7] M. Lindgren and J. Svensson, "Control of a voltage source converter connected to the grid through an LCL-filter-application to active damping," *Record. 29th Annual IEEE Power Electronics Specialists Conference, 1998. PESC 98*, vol.1, pp.229-235, May 1998.

[8] E. Wu and P. W. Lehn, "Digital Current Control of a Voltage Source Converter with Active Damping of LCL Filter Resonance," *IEEE Trans. on Power Electron.*, vol. 21, pp. 1364-1373, Sept. 2006.
[9] J. Dannehl, M. Liserre and F.W. Fuchs, "Filter-Based Active Damping of Voltage Source Converters With LCL Filter," *IEEE Trans. on Ind. Electron.*, vol. 58, pp. 3623-3633, Aug. 2011.
[10] J. Dannehl, F.W. Fuchs, S. Hansen and P.B. Thøgersen, "Investigation of Active Damping Approaches for PI-Based Current Control of Grid-Connected Pulse Width Modulation Converters With LCL Filters," *IEEE Trans. on Ind. Electron.*, vol. 46, pp. 1509-1517, July 2010.
[11] D. Pan, X. Ruan, C. Bao, W. Li and X. Wang, "Capacitor-Current-Feedback Active Damping With Reduced Computation Delay for Improving Robustness of LCL-Type Grid-Connected Inverter," *IEEE Trans. on Power Electron.,* vol.29, no.7, pp.3414-3427, July 2014.
[12] A. Draou, Y. Sato and T. Kataoka "A new state feedback based transient control of PWM AC to DC Voltage type converter," *IEEE Trans. on Power Electron.*, vol. 10, pp. 716-724, Nov. 1995.
[13] X. Mingyu, Z. Yu, K. Yong, Y. Yongxian, L. Shuming and L. Fangrui, "Full Feedforward of Grid Voltage for Discrete State Feedback Controlled Grid-Connected Inverter With LCL Filter," *IEEE Trans. on Ind. Electron.*, vol. 27, pp. 4234-4247, Oct. 2012.
[14] J. Dannehl and F.W. Fuchs, "PI State Space Current Control of Grid-Connected PWM Converters With LCL Filters," *IEEE Trans. on Ind. Electron.*, vol. 25, pp. 2320-2330, Sept. 2010.
[15] C. Ramos, A. Martins and A. Carvalho, "Complex state-space current controller for grid-connected converters with an LCL filter," *35th Annual Conference of IEEE Ind. Electron., 2009. IECON '09.*, pp. 296-301, 2009.
[16] T. Hao, Z. Rongxiang, T. Shengqing and Z. Zheng, "Linear quadratic optimal control of a single-phase grid-connected inverter with an LCL filter," *2012 IEEE International Symposium Industrial Electronics (ISIE)*, p. 372-376, 2012.
[17] X. Mingyu, Z. Yu, L. Fangrui, K. Yong and Y. Yongxian, "Optimized pole and zero placement with state observer for LCL-type grid-connected inverter," *IEEE Energy Conversion Congress and Exposition (ECCE)*, p. 377-382, 2011.
[18] J.R. Massing, H. Pinheiro, V.F. Montagner and R.C.L.F. Oliveira, "Robust current control of grid-connected converters with LCL-filter," *in Brazilian Power Electronics Conference (COBEP)*, pp. 244-248, 2011.
[19] N. Hoffmann, F.W. Fuchs, "Minimal Invasive Equivalent Grid Impedance Estimation in Inductive-Resistive Power-Networks using Extended Kalman-Filter," *IEEE Trans. on Ind. Electron.*, vol. 29, pp. 631-641, Feb. 2014.
[20] I.J. Gabe, J.R. Massing, V.F. Montagner and H. Pinheiro, "Stability analysis of grid-connected voltage source inverters with LCL-filters using partial state feedback," *European Conference on Power Electronics and Applications*, pp. 1-10, 2007.
[21] J.R. Massing, M. Stefanello, H.A. Grundling and H. Pinheiro, "Adaptive Current Control for Grid-Connected Converters With LCL Filter," *IEEE Trans. on Ind. Electron.*, vol. 59, pp. 4681-4693, Dec. 2012.
[22] M. B. Lindgren, "Feedforward-Time Efficient Control of a Voltage Source Converter connected to the grid by lowpass filters," *Power Electronics Specialists Conference (PESC),* June 1995.
[23] B. Bolsens, K. De Brabandere, J. Van den Keybus, J. Driesen and R. Belmans, "Model-based generation of low distortion currents in grid-coupled PWM-inverters using an LCL output filter," *IEEE Trans. on Ind. Electron.*, vol. 21, pp. 1032-1040, July 2006.
[24] N. Hoffmann, M. Hempel, and M.C. Harke, "F.W. Fuchs "Observer-based grid voltage disturbance rejection for grid connected voltage source PWM converters with line side LCL filters," *IEEE Energy Conversion Congress and Exposition (ECCE)*, pp.69-76, 2012.
[25] M. Cespedes and J. Sun, "Adaptive Control of Grid-Connected Inverters Based on Online Grid Impedance Measurements," *IEEE Trans. on Sustain. Energy,* vol.5, no.2, pp.516-523, April 2014.
[26] I. J. Gabe, V. F. Montagner, H. Pinheiro, "Design and Implementation of a Robust Current Controller for VSI Connected to the Grid Through an LCL Filter," *IEEE Trans. Ind. Electron.*, vol. 24, pp. 1444-1452, June 2009.
[27] M. Sumner, B. Palethorpe, D.W.P. Thomas, P. Zanchetta and M.C. Di Piazza, "A technique for power supply harmonic impedance estimation using a controlled voltage disturbance," *IEEE Trans. Ind. Electron.*, vol. 17, pp. 207-215, Mar. 2002.
[28] G. Ellis, "*Observer in Control Systems", Academic Press, 2002*, p. 121.
[29] A.G. Yepes, F.D. Freijedo, J. Doval-Gandoy, O. López, J. Malvar and P. Fernandez-Comesaña, "Effects of Discretization Methods on the Performance of Resonant Controllers," *IEEE Trans. on Ind. Electron.*, vol. 25, pp. 1692-1712, July 2010.